Ultracold bosons in disordered superlattices: Mott insulators induced by tunneling

D. Muth, A. Mering, and M. Fleischhauer
Fachbereich Physik, Technische Universität Kaiserslautern, D-67663 Kaiserslautern, Germany
(Received 22 February 2008; published 15 April 2008)

We analyze the phase diagram of ultracold bosons in a one-dimensional superlattice potential with disorder, using the time-evolving block decimation algorithm for infinite-sized systems. For degenerate potential energies within the unit cell of the superlattice, loophole-shaped insulating phases with noninteger filling emerge with a particle-hole gap proportional to the boson hopping. Addition of a small amount of disorder destroys this gap. For not too large disorder, the loophole Mott regions detach from the axis of vanishing hopping, giving rise to insulating islands. Thus the system shows a transition from a compressible Bose glass to a Mott-insulating phase with increasing hopping amplitude. We present a straightforward effective model for the dynamics within a unit cell which provides a simple explanation for the emergence of Mott-insulating islands. In particular, it gives rather accurate predictions for the inner critical point of the Bose glass to Mott insulator transition.

DOI: 10.1103/PhysRevA.77.043618 PACS number(s): 03.75.Lm, 73.43.Nq, 03.75.Hh

I. INTRODUCTION

Ultracold atomic gases in light-induced periodic potentials have become an important experimental testing ground for concepts of solid-state and many-body physics, since they allow the realization of precisely controllable model Hamiltonians with widely tunable parameters. This development was triggered by the theoretical proposal of Jaksch *et al.* [1] that ultracold bosonic atoms in an optical lattice are well described by the Bose-Hubbard model and the subsequent observation of the superfluid–Mott-insulator transition in that system by Greiner *et al.* [2]. A characteristic feature of light-induced periodic potentials is the possibility to modify their properties in a simple way. For example, when phase-locked lasers with different but commensurable frequencies are superimposed to create a periodic dipole potential, different types of superlattices with more complex unit cells can be constructed [1,3–9]. Superimposed optical lattices with noncommensurate frequencies furthermore mimic a disordered potential [10].

In the present paper we study the phase diagram of ultracold bosons in a one-dimensional superlattice potential with degenerate potential energies and/or degenerate tunneling rates within the unit cell. For such a system loophole-shaped Mott-insulator domains with fractional filling have been predicted by Buonsante, Penna, and Vezzani [8] within a multiple-site mean-field approach, as well as with a cell strong-coupling perturbation approach [9]. In contrast to the Mott lobes at integer filling known from the simple Bose-Hubbard model, which exist also in the superlattice, the characteristic feature of the loophole insulators is a particle-hole gap that vanishes at zero boson hopping J. So in the μ-J phase diagram, where μ is the chemical potential, these domains touch the $J=0$ line only at a single point. We here perform numerical simulations using the time-evolving block decimation algorithm (TEBD) introduced by Vidal [11] in the infinite-system variant (iTEBD) [12], as well as density matrix renormalization group (DMRG) calculations [13], to determine the boundaries of the different Mott-insulating regions in the phase diagram. We also present a simple effective model that provides a straightforward explanation for the emergence of the loophole insulators by taking into account hopping processes between the sites of degenerate potential energy within a unit cell but neglecting tunneling between different unit cells.

We then study the influence of some additional disorder potential with continuous, bounded distribution. If the maximum amplitude of the disorder is not too large, the Mott lobes shrink in a similar way as for the simple Bose-Hubbard model [14]. The loophole Mott domains also shrink. As a consequence, near the critical (fractional) filling, Mott-insulating islands emerge surrounded by a Bose-glass phase. A rather peculiar property of this system is the phase transition from a compressible (Bose-glass) phase for small values of the bosonic hopping J to an incompressible Mott phase for larger tunneling rates, i.e., we have a tunneling-induced Mott insulator. The effective model describing the full dynamics within a unit cell provides a simple explanation for this and gives good quantitative predictions for the critical value J_c for the compressible-phase to Mott-insulator transition. The analytical predictions are compared to numerical simulations again using the iTEBD algorithm for a superlattice with disorder.

II. THE MODEL

We consider ultracold bosonic atoms in an optical superlattice, having a periodic structure with a period l of some lattice sites. As shown in [1], the physics of these atoms can be described by the so called superlattice Bose-Hubbard model (BHM), extensively studied in [7–9,15]. We here work mostly in the grand canonical BHM; only the calculations of the shape of the loophole insulators in Secs. III B and IV A will be performed for fixed particle numbers. In second quantization, the BHM reads as

$$\hat{H} = -J\sum_j t_j(\hat{a}_j^\dagger \hat{a}_{j+1} + \hat{a}_{j+1}^\dagger \hat{a}_j) + \frac{U}{2}\sum_j \hat{n}_j(\hat{n}_j - 1) - \sum_j (\mu - v_j)\hat{n}_j, \quad (1)$$

where $\hat{a}_j$ and $\hat{a}_j^\dagger$ are the annihilation and creation operators of

the bosons at lattice site j, and $\hat{n}_j=\hat{a}_j^\dagger\hat{a}_j$ is the corresponding number operator. The particles can tunnel from one lattice site to a neighboring one with hopping rate J, t_j accounts for the variation of the hopping due to the superlattice potential, v_j accounts for local variations of the potential energy within a unit cell, and μ is the (global) chemical potential.

A particularly interesting situation arises if there is a degeneracy in the tunneling amplitudes and local potentials within the unit cell. This will be studied in detail in the following. For simplicity we focus on a special superlattice structure in which only the local potential is varied with period 3, namely,

$$\boldsymbol{v}=\{v_1,v_1,v_2\} \tag{2}$$

with $v_1-U<v_2<v_1<U$ and $\boldsymbol{t}=\{1,1,1\}$. It should be noted that the results obtained for this case are qualitatively identical to the more general case $\boldsymbol{t}=\{t_1,t_1,t_2\}$ and $\boldsymbol{v}=\{v_1,v_1,v_2\}$.

III. SUPERLATTICE WITHOUT DISORDER

Let us consider first a superlattice BHM without disorder in the two cases $\boldsymbol{v}=\{\frac{U}{2},\frac{U}{2},0\}$, $\boldsymbol{t}=\{1,1,1\}$, and $\boldsymbol{v}=\{0,0\}$, $\boldsymbol{t}=\{1,0.2\}$. As shown in Ref. [9], within a supercell mean-field approach such superlattices lead to loophole-shaped insulator phases at fractional bosonic filling. In the following we will determine the boundaries of these loophole phases numerically and compare them to the mean-field predictions. Furthermore, we will present a rather simple model which provides an intuitive explanation.

A. Numerical results

In order to calculate the boundaries of the Mott phases for the superlattice Bose-Hubbard model, we apply the iTEBD algorithm as described in the Appendix to calculate the ground state of Hamiltonian (1). We are able to calculate properties such as the local density $\rho=\overline{\langle n\rangle}$ as a function of J and μ. Using this method to map out the shape of the insulating regions, we make use of the fact that for any Mott phase the average local density is an exact multiple of $1/l$, l being the period of the superlattice. Thus the phase boundaries can be well approximated by the line where

$$\mu_{\mathrm{cr}}=\mu(\overline{\langle n\rangle}) \quad \text{where } \overline{\langle n\rangle}=m/l\pm\varepsilon \tag{3}$$

for some $m\in\mathbb{N}$ (indicating the order of the lobe) and some $1/l\gg\varepsilon>0$ [16]. This line can be calculated by finding the value of μ using a bisection method for a set of given m and J. Figures 1 and 2 show the results of this approach for the two different superlattice potentials specified above.

The phase diagrams consist of a number of incompressible Mott phases, separated by a superfluid region. In contrast to the BHM for a simple lattice, there are, however, two types of insulating phase: The lobe-shaped ones, well known from the simple-lattice Bose-Hubbard model, which have a finite extent at $J=0$, and the loophole-shaped ones, which vanish at $J=0$. In general there are l distinct insulating regions for a superlattice of period l. A loophole is present, whenever the local potential v_j is the same for two sites in the same unit cell. The following section will give a qualitative understanding of these loophole Mott regions.

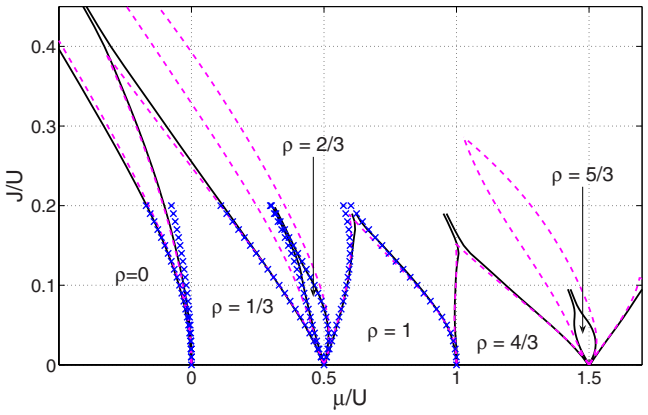

FIG. 1. (Color online) Incompressible phases for an $l=3$ superlattice with $\boldsymbol{v}=\{U/2,U/2,0\}$ and $\boldsymbol{t}=\{1,1,1\}$ without disorder. Solid line, iTEBD; crosses, DMRG; dashed line, CSCPE from [9]. Simulation parameters for the iTEBD are $\chi=5$, $D-1=3$, $\beta/U=1000$ (see the Appendix for definitions). DMRG results are obtained from an infinite-size extrapolation.

Figure 1 shows our results in the case $\boldsymbol{v}=\{\frac{U}{2},\frac{U}{2},0\}$, $\boldsymbol{t}=\{1,1,1\}$, together with the cell strong-coupling pertubative expansion (CSCPE) results from [9]. As a check of our numerics we added numerical results from a density matrix renormalization group calculation [13]. The existence of noninteger insulating phases at $J=0$ in this special superlattice has a direct connection to the case of a binary disorder BHM [17], which arises, for example, in the presence of a second, immobile particle species (here of filling $\frac{1}{3}$ with an interspecies interaction of $v=-\frac{U}{2}$).

Figure 2 shows the numerical results for the case of a $v=\{0,0\}$ and $t=\{1,0.2\}$ superlattice of period 2 together with the quantum Monte Carlo (QMC) results and the CSCPE

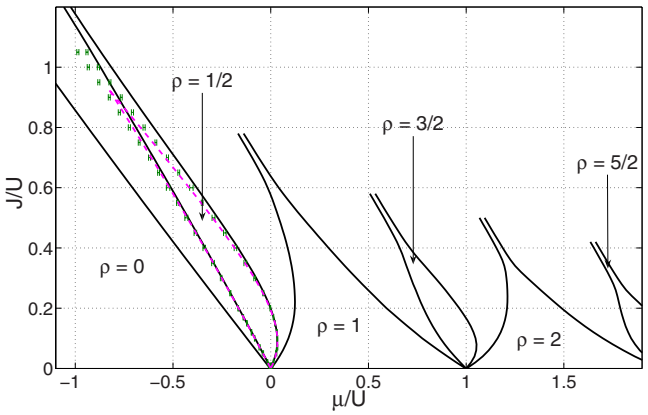

FIG. 2. (Color online) Incompressible phases for an $l=2$ superlattice with $\boldsymbol{v}=\{0,0\}$ and $\boldsymbol{t}=\{1,0.2\}$ without disorder. Solid line, iTEBD; crosses with error bars, QMC (only for $\varrho=1/2$); and dashed line, CSCPE (only for $\varrho=1/2$), both from [9]. Simulation parameter for the iTEBD are $\chi=7$, $D-1=4$ for $\rho<2$ and $D-1=5$ for $\rho\geq 2$, $\beta/U=1000$ (see the Appendix for definitions). For some phase boundaries ε was set to 0.02 instead of 0.005 in order to avoid numerical artifacts.

data from [9]. The agreement between our numerics and the CSCPE is naturally good for small J but deteriorates for larger J. It is also apparent that, while the insulator lobes are rather well described by the CSCPE approach, it is much less accurate for the loophole insulator regions, in particular for the case of varying potential depth (see Fig. 1).

B. Two-site model

We will argue in the following that the loophole insulator phases can entirely be understood from the effective dynamics within a unit cell of the superlattice using a simplified version of the zeroth-order CSCPE from [9]. To this end let us discuss the above situation, where $\boldsymbol{v}=\{v_1,v_1,v_2\}$, with $v_2<v_1$.

The presence of Mott lobes at fractional filling with a finite extent at $J=0$ can easily be understood along the lines of the simple-lattice BHM. As long as the filling is less than $\frac{1}{3}$, the particles will occupy sites with local potential v_2. Thus the chemical potential reads

$$\mu_{1/3}^{-}=v_2. \tag{4}$$

When the filling reaches the value $\frac{1}{3}$ additional particles will start to occupy sites with local potential v_1, giving rise to a particle-hole gap,

$$\Delta\mu_{1/3}=\mu_{1/3}^{+}-\mu_{1/3}^{-}=v_1-v_2. \tag{5}$$

To explain the existence of the loophole insulators, one has to take into account a finite hopping J. For $J=0$ any particle added to the system between $\rho=\frac{1}{3}$ and 1 increases the total energy by the same amount v_1. Thus the chemical potential stays the same. This picture changes, however when a small but finite tunneling is included. If the filling exceeds the value $\frac{1}{3}$, additional particles experience an effective superlattice potential $\boldsymbol{v}=\{v_1,v_1,U+v_2\}$, where the last term results from the interaction with particles already occupying sites with v_2. If $U>v_1-v_2$ the superlattice effectively separates into degenerate double-well problems each corresponding to a unit cell. Due to the degeneracy of the double well, any small tunneling J within the unit cell of the lattice needs to be taken into account while intracell tunneling can be ignored. A finite tunneling lifts the degeneracy of the single-particle states within the unit cell and leads to a splitting between symmetric and antisymmetric superpositions proportional to J. As long as the filling is less than $\rho=\frac{2}{3}$, the particles occupy all sites with the smallest local potential v_2 and the symmetric superposition of the double well $\{v_1,v_1\}$. After that, additional particles have to go either to an already occupied side with potential v_2, which is, however, suppressed by the large repulsive particle-particle interaction, or to the antisymmetric superposition state. The latter requires an energy on the order of v_1+J, thus leading to another particle-hole gap on the order of J induced by intracell tunneling. More quantitatively the gap can be calculated by diagonalizing the two-site Hamiltonians $\mathcal{H}(N_B)$ for zero, one, or two particles, (i.e., $N_B=0,1,2$), which read

$$\mathcal{H}(0)=0 \tag{6}$$

in the basis $\{|00\rangle\}$,

$$\mathcal{H}(1)=\begin{bmatrix} v_1 & -J \\ -J & v_1 \end{bmatrix} \tag{7}$$

in the basis $\{|10\rangle,|01\rangle\}$, and

$$\mathcal{H}(2)=\begin{bmatrix} U+2v_1 & -J\sqrt{2} & 0 \\ -J\sqrt{2} & 2v_1 & -J\sqrt{2} \\ 0 & -J\sqrt{2} & U+2v_1 \end{bmatrix} \tag{8}$$

in the basis $\{|20\rangle,|11\rangle|02\rangle\}$. The resulting ground state energies are given by

$$E(0)=0, \tag{9}$$

$$E(1)=v_1-J, \tag{10}$$

$$E(2)=\frac{1}{2}(U+4v_1-\sqrt{16J^2+U^2}). \tag{11}$$

Calculating the chemical potentials $\mu_{2/3}^{+}=E(2)-E(1)$ and $\mu_{2/3}^{-}=E(1)-E(0)$ yields

$$\mu_{2/3}^{-}=v_1-J, \tag{12}$$

$$\mu_{2/3}^{+}=J+v_1+\frac{U}{2}-\frac{1}{2}\sqrt{16J^2+U^2}, \tag{13}$$

$$=v_1+J+O(J^2), \tag{14}$$

giving rise to a particle-hole gap

$$\Delta\mu_{2/3}=J+O(J^2). \tag{15}$$

A generalization of this discussion to the case of higher-order loophole insulators or larger supercells is straightforward. For higher-order loopholes, the accuracy becomes better, since the difference in the chemical potential between the rightmost and the other sites scales as $U(n-1)$, where $n=\lfloor\frac{m}{l}\rfloor+1$ is the number of particles of the corresponding Mott-insulating lobe. This means that the effective two-site model gets even better for higher fillings. Qualitatively, one can understand the change in the shape of the loopholes for higher order (also see Fig. 5) just by considering the replacement $J\to(n+1)J$ in (7), because the single-particle matrix $\mathcal{H}(1)$ is the only one relevant for the linear part of (15) and because this replacement is the only influence of the other bosons already filling the lattice on the hopping in $\mathcal{H}(1)$.

IV. SUPERLATTICE WITH DISORDER

We now include a small disorder to the superlattice Bose-Hubbard model. Of particular interest is the effect of the disorder on the loophole insulator phases. Disorder can be incorporated into the model by replacing the last part of (1) according to

$$-\sum_j(\mu-v_j)\hat{n}_j\to-\sum_j(\mu-v_j+\Delta_j)\hat{n}_j \tag{16}$$

with Δ_j being independent random numbers with continuous and bounded distribution, $\Delta_j\in[-\Delta,\Delta]$. In the following we

will restrict our analysis to the case of the superlattice potential $\boldsymbol{v}=\{\frac{U}{2},\frac{U}{2},0\}$, $\boldsymbol{t}=\{1,1,1\}$ and consider a canonical ensemble.

A. Two-site model with disorder

If the disorder is small, i.e., if $3\Delta<U+2v_2-v_1$, the properties of the system in the vicinity of the $\Delta=0$ loophole insulators can again be understood by considering the unit cell only, i.e., within an effective two-site model. The $\Delta=0$ loophole insulator can be characterized by the number of particles per two-site cell, $2n-1$, and the disorder-modified chemical potential $\mu=\{v_1+\Delta_1,v_1+\Delta_2\}$.

Defining the total local energy in one unit cell as

$$T_{n_1,n_2}:=\frac{U}{2}n_1(n_1-1)+\frac{U}{2}n_2(n_2-1)+\Delta_1 n_1+\Delta_2 n_2, \tag{17}$$

the two-site Hamiltonians can be written as

$$\mathcal{H}_n(2n-2)=T_{n-1,n-1}, \tag{18}$$

in the basis $\{|n-1,n-1\rangle\}$ for one particle less,

$$\mathcal{H}_n(2n-1)=\begin{bmatrix} T_{n-1,n} & -nJ \\ -nJ & T_{n,n-1} \end{bmatrix}, \tag{19}$$

in the basis $\{|n-1,n\rangle,|n,n-1\rangle\}$ for zero extra particles, and

$$\mathcal{H}_n(2n)=\begin{bmatrix} T_{n+1,n-1} & -J\sqrt{n(n+1)} & 0 \\ -J\sqrt{n(n+1)} & T_{n,n} & -J\sqrt{n(n+1)} \\ 0 & -J\sqrt{n(n+1)} & T_{n-1,n+1} \end{bmatrix} \tag{20}$$

in the basis $\{|n+1,n-1\rangle,|n,n\rangle,|n-1,n+1\rangle\}$ for one additional particle.

The breaking of the Mott insulator is determined by the particle-hole excitation with the smallest energy difference throughout the whole system. Since in our approximation all two-site cells are decoupled, one therefore has to find the configuration $\{\Delta_1,\Delta_2\}$ which minimizes the energy gap within the two-site part of the superlattice unit cell. Therefore one has to calculate the chemical potentials

$$\mu^+_{3n-1/3}=\min_{\Delta_1,\Delta_2}[E_{2n}(\Delta_1,\Delta_2)-E_{2n-1}(\Delta_1,\Delta_2)], \tag{21}$$

$$\mu^-_{3n-1/3}=\max_{\Delta_1,\Delta_2}[E_{2n-1}(\Delta_1,\Delta_2)-E_{2n-2}(\Delta_1,\Delta_2)] \tag{22}$$

that give the smallest energy lost in adding a particle and the largest energy gain in removing a particle. Using Eqs. (18) and (19) it is easy to see that the energy gap for the hole excitation $\mu^-_{3n-1/3}$ is given by

$$\mu^-_{3n-1/3}=\max_{\Delta_1,\Delta_2}\left(U(n-1)+\frac{1}{2}(\Delta_1+\Delta_2)-\frac{1}{2}\sqrt{4J^2n^2+(\Delta_1-\Delta_2)^2}\right), \tag{23}$$

which is easily seen to be maximized by $\Delta_1=\Delta_2=+\Delta$. The energy gap of a hole excitation is given by

$$\mu^-_{3n-1/3}=U(n-1)-nJ+\Delta. \tag{24}$$

In the case of a particle excitation, an analytical calculation is more involved. But in this case we can argue physically: If the disorder is $\Delta_1=\Delta_2=-\Delta$ then the energy required to add another particle is minimized because the energy of the added particle resulting from the local disorder potential is minimal, the interaction is minimal because the two particles can distribute equally on both sides, and the kinetic energy is smallest as well due to the maximal delocalization. This can be verified by a straightforward numerical minimization of (21). Using this, the energy gap of a particle excitation reads

$$\mu^+_{3n-1/3}=U\left(n-\frac{1}{2}\right)+nJ-\Delta-\frac{1}{2}\sqrt{8J^2n(n+1)+U^2}. \tag{25}$$

In order to calculate the critical tunneling rate at which the loophole insulator emerges, one needs to solve the equation

$$\mu^-_{3n-1/3}=\mu^+_{3n-1/3}. \tag{26}$$

The solution can easily be found and reads

$$J_1=\Delta\frac{U-2\Delta}{U-4\Delta} \tag{27}$$

for $n=1$, and

$$J_n=-\frac{1}{2n(n-1)}[(U-4\Delta)n-\sqrt{n^2(U^2-4U\Delta+8\Delta^2)-4\Delta(U-2\Delta)n}] \tag{28}$$

for $n>1$. In both cases, the leading terms are given by

$$J_n(\Delta)=\frac{1}{n}\Delta+\frac{n+1}{n^2}\Delta^2+O(\Delta^3), \tag{29}$$

showing that the loophole decouples from the $J=0$ axis in the presence of disorder, resulting in an insulating island. It should be noted that the two-site model cannot be used to calculate the maximum value of J for which the loophole insulator exists since, for the vanishing of the gap at large J values, intercell tunneling processes also need to be taken into account.

B. Numerical results

As seen above from the effective two-site model, the loophole insulator regions are decoupled from the $J=0$ axis giving incompressible islands. Although the system is for any given disorder realization not translationally invariant, the iTEBD method can be used also in this case. To this end we define *supercells* each of which has the same disorder. The supercells have to be large enough such that effects from spatial correlations and finite size can be ignored. We have chosen a supercell length of 96. Increasing this length did not give any noticeable changes. To calculate the physical quantities, the numerical results have to be averaged over a number of different disorder realizations, namely, over different sets of disorder $\boldsymbol{\Delta}=\{\Delta_1,\Delta_2,\ldots,\Delta_l\}$ with $\Delta_j\in[-\Delta,\Delta]$, where

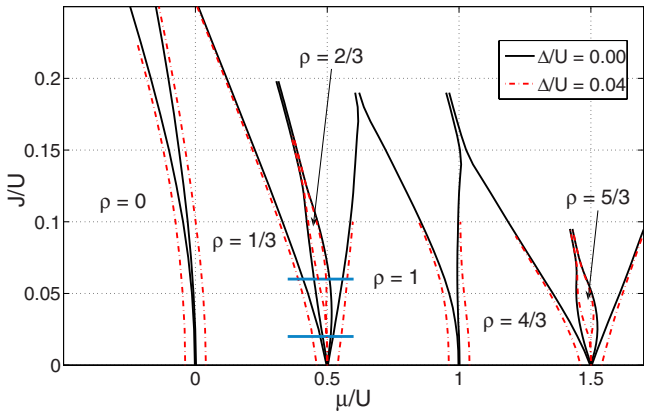

FIG. 3. (Color online) iTEBD results for boundaries of incompressible phases for $l=3$ superlattice with $\boldsymbol{v}=\{U/2,U/2,0\}$ and $\boldsymbol{t}=\{1,1,1\}$ and a disorder amplitude $\Delta/U=0.04$. Dashed line, pure case; solid line, disordered case. For simulation parameters see Fig. 1. Horizontal lines indicate the positions of density cuts of Fig. 4.

a boxed disorder distribution is assumed. The length of the vector $\boldsymbol{\Delta}$ is the same as the size of the system simulated (see the Appendix). It turns out that 20 realizations provide sufficient convergence for the purpose of this paper.

Figure 3 shows the results of the iTEBD calculations in both the pure ($\Delta=0$) and the disordered ($\Delta=0.04U$) cases. The first thing to notice is the shrinking of the Mott-insulating lobes for $J=0$ due to the disorder. As known from the BHM [14,18], the Mott lobes shrink by an amount of 2Δ at the $J=0$ axis. The second and more important thing to notice is the decoupling of the loophole insulator from the $J=0$ axis, meaning that there is no insulating phase for the corresponding filling for $J<J_{\mathrm{crit}}$, in full agreement with Eqs. (27) and (28).

The decoupling of the loophole insulator from the $J=0$ axis can most easily be seen in a cut parallel to the μ axis for fixed J, showing the average local density as a function of the chemical potential. In the case of small hopping without disorder, this cut shows, besides the expected Mott lobes at $\varrho=\frac{1}{3}$ and 1, an intermediate plateau at filling $\frac{2}{3}$, corresponding to the loophole phase (Fig. 4, lower plot, solid line). For larger hopping (upper plot, solid line), the width of the plateau is slightly increased according to the shape of the loophole in Fig. 1. In the case of disorder, the plateau for $\varrho=\frac{2}{3}$ vanishes for small hopping (Fig. 4, lower plot, dashed line). For large hopping (upper plot, dashed line), the incompressible phase survives, but with a greatly reduced width compared to the pure case, which shows the decoupling of the loophole from the $J=0$ axis as predicted.

In Fig. 5 we show the numerical results for the first, second, and third loopholes for increasing values of the normalized disorder amplitude. It should be noted that, due to the finite number of disorder realizations, it is difficult to accurately determine the lower tip of the insulating island in the numerics. In Fig. 6 we compare the onset of the insulating loopholes obtained from the analytic two-site model with numerical results. One immediately recognizes two things: First, the onset of the loophole, J_{crit}, is a monotonic function of Δ and, second, the higher the filling of the lobe, the earlier

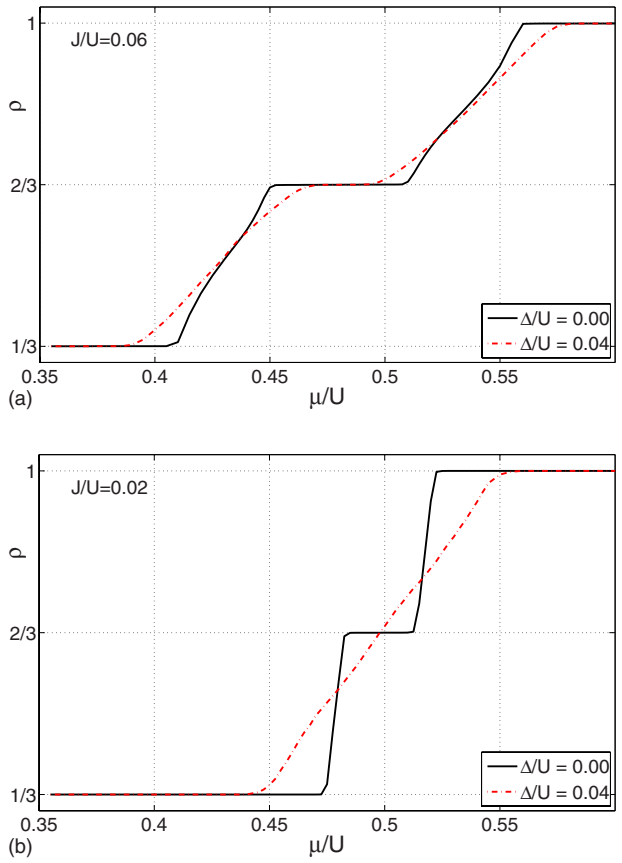

FIG. 4. (Color online) Density cut along the horizontal lines in Fig. 3 for the pure (solid line) and the disordered ($\Delta/U=0.04$, dashed line) cases. Upper plot: cut along the upper line in Fig. 3 at $J/U=0.06$; lower plot: cut along the lower line in Fig. 3 at $J/U=0.02$. Simulation parameters as in Fig. 1.

the insulating region arises. The numerical value of J_{crit} was obtained by reading off the values from the numerically determined phase diagram assuming generous error margins [19]. Taking into account these errors, Fig. 6 shows a rather

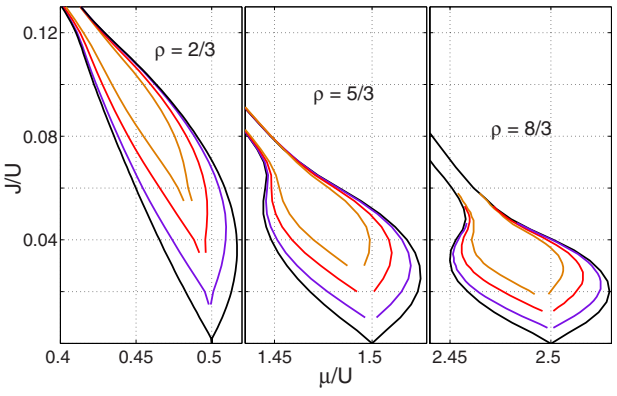

FIG. 5. (Color online) Detailed analysis of the first three loophole insulators (from left to right: $\varrho=2/3$, 5/3, and 7/3) with varying disorder amplitude, increasing from the outer to the inner lines (black, $\Delta/U=0.00$; magenta, $\Delta/U=0.02$; red, $\Delta/U=0.04$; orange, $\Delta/U=0.06$). For the simulation parameters, see Fig. 1 except for $D-1=4$ in the rightmost plot ($\varrho=8/3$).

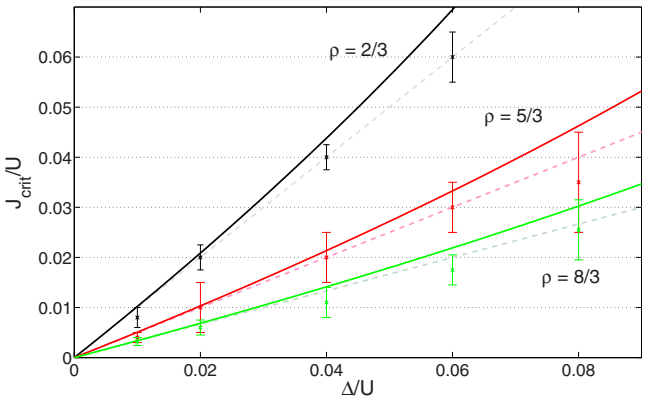

FIG. 6. (Color online) Critical point J_n of the onset of the loophole insulating island as a function of the disorder. Solid line, analytic prediction from Eqs. (27) and (28); crosses, data with error bars as read from Fig. 5 (not all used data are shown in Fig. 5); dashed lines, leading order in Eq. (29). From top to bottom, $n=1$, 2, and 3.

good agreement of the two-site model with the numerics. However, the analytic prediction tend to be slightly too large compared to the numerics; nevertheless giving the right leading order for small Δ. This is because for larger Δ the critical hopping gets larger than allowed by the assumption of a decoupled two-site problem. By diagonalizing the complete three-site unit cell with periodic boundary conditions, which gives another but less intuitive approximation, we get a curve for J_{crit} that is below the two-site prediction, but is the same in first order and in better agreement with our numerics.

V. SUMMARY

In the present paper we have analyzed the superlattice Bose-Hubbard model with and without disorder. In particular, the cases of degenerate potential energies and/or degenerate tunneling rates within the unit cell of the superlattice have been discussed. Using both exact numerical methods such as the infinite-size time evolving block decimation algorithm and the density matrix renormalization group, we calculated the boundaries of incompressible Mott-insulating phases. The existence of additional loophole-shaped Mott domains, predicted before, was verified, and their numerically determined phase boundaries compared to other approaches such as the cell strong-coupling expansion. A simple effective model was presented that takes the full dynamics within a unit cell into account. The model provides a rather straightforward explanation for the emergence of loophole Mott domains in the case without disorder. Adding a small amount of disorder with continuous, bounded distribution leads to a shrinking of the loopholes to Mott-insulating islands with the remarkable feature of a compressible-phase to insulating transition with increasing bosonic hopping. The analytic predictions for the critical hopping for this transition from the effective model were compared to numerical simulations and found in very good agreement.

ACKNOWLEDGMENTS

The authors would like to thank P. Buonsante for providing the CSCPE and QMC data for the superlattice without disorder. We also thank U. Schollwöck for support with the DMRG calculations. Financial support by the DFG through the SFB-TR 49 and the GRK 792 is gratefully acknowledged. Also most of the DMRG calculations have been performed at the John von Neumann–Institut für Computing, Forschungszentrum Jülich.

APPENDIX: THE TEBD ALGORITHM AND THE ITEBD IDEA

In the following we give a short summary of the numerical algorithm used in Secs. III A and IV B. The basic idea of the TEBD algorithm emerged from quantum-information theory [11] and it can be used to simulate one-dimensional quantum computations that involve only a limited amount of entanglement.

Here we want to use it for an imaginary time evolution of the one-dimensional Bose-Hubbard model. The state of the system can be represented as a matrix product state:

$$|\Psi\rangle = \sum_{\alpha_1,\alpha_2,\ldots,\alpha_L=1}^{\chi} \sum_{i_1,i_2,\ldots,i_L=0}^{D} \Gamma^{[1]i_1}_{\alpha_1} \lambda^{[1]}_{\alpha_1} \Gamma^{[2]i_2}_{\alpha_1\alpha_2} \cdots \lambda^{[L-2]}_{\alpha_{L-2}} \times \Gamma^{[L-1]i_{L-1}}_{\alpha_{L-2}\alpha_{L-1}} \lambda^{[L-1]}_{\alpha_{L-1}} \Gamma^{[L]i_L}_{\alpha_{L-1}} |i_1 \cdots i_L\rangle. \tag{A1}$$

Here D is the dimension of the local Hilbert space on a single site and χ is the number of basis states in the Schmidt decompositions (see below) to be taken into account. χ is a measure for the maximum entanglement in the system and is assumed not to increase with system size or to increase only very slowly. In our model the number of particles per site is in principle not bounded. But to reduce the numerical effort one can safely set a maximum number of particles, $D-1$, allowed per site, since higher occupancies are strongly suppressed due to the on-site interaction. $|i_1 \cdots i_L\rangle$ is the state from the Fock basis, where there are i_k bosons on site k.

Furthermore, we require our matrix product representation to be in the *canonical* form, i.e., Eq. (A1) represents the Schmidt decomposition for any bipartite splitting of the system at the same time. This means that, for any given k, the Schmidt decomposition between sites k and $k+1$ is given by

$$|\Psi\rangle = \sum_{\alpha=1}^{\chi} \lambda^{[k]}_{\alpha} |\Psi^{[1,\ldots,k]}_{\alpha}\rangle |\Psi^{[k+1,\ldots,L]}_{\alpha}\rangle, \tag{A2}$$

where the Schmidt coefficients $\lambda^{[k]}_{\alpha}$ are normalized as

$$\sum_{\alpha=1}^{\chi} \lambda^{[k]2}_{\alpha} = 1, \tag{A3}$$

and the $\{|\Psi^{[1,\ldots,k-1]}_{\alpha}\rangle\}_{\alpha}$ ($\{|\Psi^{[k,\ldots,L]}_{\alpha}\rangle\}_{\alpha}$) form an orthonormal set of states in the subspace of the first k (last $L-k$) sites. By sorting the Schmidt coefficients in nonascending order for every bond, this makes the representation *de facto* unique. Explicitly,

$$|\Psi_\alpha^{[1,\ldots,k]}\rangle = \sum_{\substack{\alpha_1,\alpha_2,\ldots,\alpha_k \\ i_1,i_2,\ldots,i_k}} \Gamma_{\alpha_1}^{[1]i_1} \cdots \lambda_{\alpha_{k-1}}^{[k-1]} \Gamma_{\alpha_{k-1}\alpha}^{[k]i_k} |i_1 \cdots i_k\rangle, \tag{A4}$$

where the λ's account for all the Schmidt coefficients and the Λ's take care of the transformation into Fock space at every single site. Describing an arbitrary state in general requires that the Schmidt number χ is of the order D^L. We will use, however, a relatively small, constant χ to avoid exponentially increasing complexity of the numerical problem. It has been shown in [20] that this seemingly strong assumption is justified and gives a good approximation for the ground state. This is related to the fact that the ground state of one-dimensional systems with finite-range interactions either has a constant entanglement (for noncritical systems) or the entanglement increases only logarithmically with the size (for critical systems). Small values of χ give usually very good results for local observables, while correlations are only poorly approximated over very large distances. For the latter the approximation can be improved by choosing a larger χ, proportional to the distance [12]. The number of coefficients needed to specify the matrix product state with given fixed χ is of the order $LD\chi^2$ and can be handled numerically, in contrast to the D^L coefficients required for representation in the full Fock space.

Expressing the state in a local basis for sites k and $k+1$ only,

$$|\Psi\rangle = \sum_{\alpha,\beta,\gamma=1}^{\chi} \sum_{i,j=0}^{D} \lambda_\alpha^{[k-1]} \Gamma_{\alpha\beta}^{[k]i} \lambda_\beta^{[k]} \Gamma_{\beta\gamma}^{[k+1]j} \lambda_\gamma^{[k+1]} \times |\Psi_\alpha^{[1\ldots k-1]}\rangle |i\rangle |j\rangle |\Psi_\gamma^{[k+2,\ldots,L]}\rangle, \tag{A5}$$

we see that applying an operator that involves sites k and $k+1$ only is equivalent to manipulating the matrices $\Gamma^{[k]}$ and $\Gamma^{[k+1]}$ and the vector $\lambda^{[k]}$ only, which is implemented as follows.

For reasons of stability we use $A_{\alpha\beta}^{[k]i} := \Gamma_{\alpha\beta}^{[k]i} \lambda_\beta^{[k]}$ throughout the algorithm [21]. To shorten the notation we rename $\lambda_\alpha^{[k-1]} |\Psi_\alpha^{[1\ldots k-1]}\rangle \to |\alpha\rangle$ and $\lambda_\gamma^{[k+1]} |\Psi_\gamma^{[k+2\ldots L]}\rangle \to |\gamma\rangle$ in (A5), giving

$$|\Psi\rangle = \sum_{\substack{\alpha\gamma \\ ij}} \sum_{\beta} A_{\alpha\beta}^{[k]i} A_{\beta\gamma}^{[k+1]j} \frac{1}{\lambda_\gamma^{[k+1]}} |\alpha i j \gamma\rangle. \tag{A6}$$

Applying a two-site operator V given by the matrix V_{lm}^{ij} then results in

$$V|\Psi\rangle = |\tilde{\Psi}\rangle = \sum_{\substack{\alpha\gamma \\ ij}} \underbrace{\sum_{lm\beta} V_{lm}^{ij} A_{\alpha\beta}^{[k]l} A_{\beta\gamma}^{[k+1]m}}_{T_{\alpha\gamma}^{ij}} \frac{1}{\lambda_\gamma^{[k+1]}} |\alpha i j \gamma\rangle. \tag{A7}$$

The objective is now to decompose T into a product of matrices $\tilde{A}_{\alpha\beta}^{[k]i} \tilde{A}_{\beta\gamma}^{[k+1]j}$ and to keep the canonical form. The $\{\tilde{A}_{\beta\gamma}^{[k+1]j}\}_\beta$ are the eigenvectors of the reduced density matrix

$$\rho^{[k+1,\ldots,L]} = \mathrm{Tr}^{[1,\ldots,k]} |\tilde{\Psi}\rangle\langle\tilde{\Psi}| = \sum_{\substack{j_1 j_2 \\ \gamma_1\gamma_2}} \underbrace{\sum_{i\alpha} \lambda_\alpha^{[k-1]2} T_{\alpha\gamma_1}^{ij_1} (T_{\alpha\gamma_2}^{ij_2})^*}_{M_{\gamma_1\gamma_2}^{j_1 j_2}} \frac{|j_1\gamma_1\rangle\langle j_2\gamma_2|}{\lambda_{\gamma_1}^{[k+1]} \lambda_{\gamma_2}^{[k+1]}}. \tag{A8}$$

Diagonalizing M gives the new $\tilde{A}_{\beta\gamma}^{[k+1]j}$ as eigenvectors and the new $(\tilde{\lambda}_\beta^{[k]})^2$ as eigenvalues. (Using the Γ matrices instead of the A matrices would require a division by $\lambda_\gamma^{[k+1]}$. But $\lambda_\gamma^{[k+1]}$ can be zero if the Schmidt number for this bond is smaller than χ.) In general there are $D\chi$ nonzero eigenvalues. (This is due to the possible creation of entanglement by V.) But we can keep the χ biggest of them. Therefor we have to renormalize the new $\lambda^{[k]}$ according to (A3). This is necessary anyway if we have a nonunitary V as in the case of an imaginary time evolution. The $\tilde{A}_{\alpha\beta}^{[k]i}$ are given by $\Sigma_{j\gamma} (\tilde{A}_{\beta\gamma}^{j})^* T_{\alpha\gamma}^{ij}$.

In order to calculate the ground state of our system (see [22]), we divide the Hamiltonian (1) into two parts $\hat{H}_{\mathrm{even}}$ and $\hat{H}_{\mathrm{odd}}$, where $\hat{H}_{\mathrm{even}}$ ($\hat{H}_{\mathrm{odd}}$) couples sites j and $j+1$ for even (odd) j only. The local parts of $\hat{H}$ can be distributed between $\hat{H}_{\mathrm{even}}$ and $\hat{H}_{\mathrm{odd}}$ arbitrarily. The ground state is then given by an imaginary time evolution

$$|\Psi_{\mathrm{ground}}\rangle = \lim_{\beta\to\infty} \frac{e^{-\hat{H}\beta}|\Psi_0\rangle}{\| e^{-\hat{H}\beta}|\Psi_0\rangle \|}. \tag{A9}$$

Here any initial state $|\Psi_0\rangle$ is sufficient, as long as it has a finite overlap with the (yet unknown) ground state. The evolution is implemented by repeatedly applying small time steps $e^{-\hat{H}\varepsilon}$, so called Trotter steps. The norm is conserved in this procedure (see above). So after T steps only the ground state has a reasonable contribution to our state if $\beta = T\varepsilon$ is much bigger than the inverse of the energy of the first excited state (relative to the ground state energy). In order to write $e^{-\hat{H}\varepsilon}$ as a product of two-site operators we use the Suzuki-Trotter decomposition [23]. In first order one can get $e^{-\hat{H}\varepsilon} = e^{-\hat{H}_{\mathrm{even}}\varepsilon} e^{-\hat{H}_{\mathrm{odd}}\varepsilon} + O(\varepsilon^2)$, and in second order $e^{-\hat{H}\varepsilon} = e^{-\hat{H}_{\mathrm{even}}/2\varepsilon} e^{-\hat{H}_{\mathrm{odd}}\varepsilon} e^{-\hat{H}_{\mathrm{even}}/2\varepsilon} + O(\varepsilon^3)$. For higher orders see [23]. Thus we can calculate the ground state by repeatedly applying two-site operators.

To calculate expectation values of observables we again take a look at (A5). The expectation value of a nearest neighbor observable, say $\langle\Psi|\hat{a}_k^\dagger \hat{a}_{k+1}|\Psi\rangle$ can be directly calculated because all occurring states are mutually orthogonal and normalized. An nth-site nearest neighbor observable can be calculated by expressing the state in the local basis for site k to $k+n$ analogously to (A5). For non-nearest-neighbor observables we can use the SWAP gate to bring the sites of interest together [11].

A powerful feature of the algorithm is its application to infinite, translationally invariant systems. Suppose a Hamiltonian that has a periodicity of c sites [as (1) has for a superlattice], restricted to $c=2$ for clarity. The state of an infinite system is a slight modification of (A1):

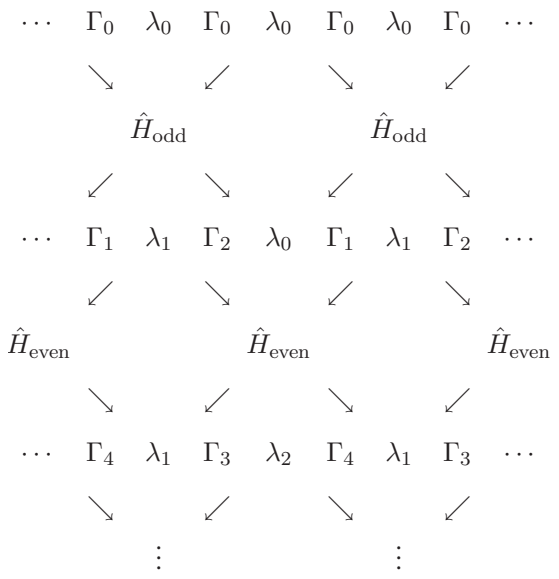

FIG. 7. Symbolic representation of the effect of the TEBD algorithm in a translationally invariant state. The uppermost (initial) state is first changed by application of H_{odd}, giving new Γ's and λ's. The second step with H_{even} then produces a list of alternating Γ's and λ's such that only two of them need to be kept in memory. Every further Trotter step preserves this symmetry.

$$|\Psi\rangle = \sum_{\substack{\alpha_{-\infty},\ldots,\alpha_{\infty} \\ i_{-\infty},\ldots,i_{\infty}}} \cdots \lambda^{[k-1]}_{\alpha_{k-1}} \Gamma^{[k]i_k}_{\alpha_{k-1}\alpha_k} \lambda^{[k]}_{\alpha_k} \times \Gamma^{[k+1]i_{k+1}}_{\alpha_k} \lambda^{[k+1]}_{\alpha_{k+1}} \cdots |i_{-\infty} \cdots i_{\infty}\rangle. \quad \text{(A10)}$$

The imaginary time evolution is started with a translationally invariant state, so all Γ's and λ's are the same in the beginning. The scheme in Fig. 7 shows that the c periodicity of the representation is preserved during real or imaginary time evolution. This is because all two-site operations $\hat{H}_{\mathrm{odd}}$ and $\hat{H}_{\mathrm{even}}$ are respectively the same and are all applied to every other pair of matrices.

So we have to store only two Γ matrices and two λ vectors. It is even more important that we only have to apply two two-site operators per Trotter step.

After imaginary time evolution we end up with a c-periodic ground state. [That means that expectation values have a periodicity of c sites, although there can be contributions in (A10) from states which have a *nonperiodic* Fock representation. This is a clear distinction from the case of periodic boundary conditions, where not only all expectation values but also the wave function must be periodic.] This is called the iTEBD algorithm [12]. It means that we can efficiently calculate observables in the thermodynamic limit. If we were using DMRG or the normal TEBD we would have to simulate large finite systems, which is time consuming, and then extrapolate to $L=\infty$ to get rid of finite-size effects but introducing additional error.

The idea works as well for $c>2$. If c is odd, we have to choose $2c$ as the period, since we need a clear distinction between $\hat{H}_{\mathrm{even}}$ and $\hat{H}_{\mathrm{odd}}$. In fact, we used it in this work for the nonperiodic Hamiltonian of the disordered superlattice model, thus not saving calculation time (a large value has to be used for c in order to have a sufficiently random disorder) but getting rid of boundary effects.

Finally we note that the TEBD algorithm itself is in principle correct only for unitary operations. Nonunitary operations were found to destroy the representation in the sense that the Schmidt vectors in are no longer exactly orthogonal, i.e., the representation is no longer canonical [24]. Additional steps to conserve orthogonality in the algorithm were proposed in [25]. These were not incorporated here, since for small ε the Trotter steps are quasiorthogonal. Numerical analysis shows that the scalar products of the normalized Schmidt vectors in the resulting ground state are of the order 10^{-3}.

[1] D. Jaksch, C. Bruder, J. I. Cirac, C. W. Gardiner, and P. Zoller, Phys. Rev. Lett. **81**, 3108 (1998).
[2] M. Greiner, O. Mandel, T. Esslinger, T. W. Hänsch, and I. Bloch, Nature (London) **415**, 39 (2002).
[3] L. Santos, M. A. Baranov, J. I. Cirac, H.-U. Everts, H. Fehrmann, and M. Lewenstein, Phys. Rev. Lett. **93**, 030601 (2004).
[4] S. Peil, J. V. Porto, B. Laburthe Tolra, J. M. Obrecht, B. E. King, M. Subbotin, S. L. Rolston, and W. D. Phillips, Phys. Rev. A **67**, 051603(R) (2003).
[5] V. G. Rousseau, M. Rigol, F. Hébert, D. P. Arovas, G. G. Batrouni, and R. T. Scalettar, Phys. Rev. B **73**, 174516 (2006).
[6] R. Roth and K. Burnett, Phys. Rev. A **68**, 023604 (2003).
[7] P. Buonsante and A. Vezzani, Phys. Rev. A **70**, 033608(R) (2004).
[8] P. Buonsante, V. Penna, and A. Vezzani, Phys. Rev. A **70**, 061603(R) (2004); P. Buonsante, V. Penna, and A. Vezzani, Laser Phys. **15**, 361 (2005).
[9] P. Buonsante and A. Vezzani, Phys. Rev. A **72**, 013614 (2005).
[10] L. Fallani, J. E. Lye, V. Guarrera, C. Fort, and M. Inguscio, Phys. Rev. Lett. **98**, 130404 (2007).
[11] G. Vidal, Phys. Rev. Lett. **91**, 147902 (2003).
[12] G. Vidal, Phys. Rev. Lett. **98**, 070201 (2007).
[13] U. Schollwöck, Rev. Mod. Phys. **77**, 259 (2005).
[14] M. P. A. Fisher, P. B. Weichman, G. Grinstein, and D. S. Fisher, Phys. Rev. B **40**, 546 (1989).
[15] P. Buonsante, V. Penna and A. Vezzani, Phys. Rev. A **72**, 031602(R) (2005).
[16] Throughout the paper we set $\varepsilon=0.005$.
[17] A. Mering and M. Fleischhauer, Phys. Rev. A **77**, 023601 (2008).
[18] J. K. Freericks and H. Monien, Phys. Rev. B **53**, 2691 (1996).
[19] Calculating the tip of a lobe is in general numerically expensive.

[20] F. Verstraete and J. I. Cirac, Phys. Rev. B **73**, 094423 (2006).
[21] The vectors $\lambda^{[k]}$ have all to be kept separately in order to not lose information about the canonical form of the state.
[22] G. Vidal, Phys. Rev. Lett. **93**, 040502 (2004).
[23] M. Suzuki, Phys. Lett. A **146**, 319 (1990).
[24] R. Orus and G. Vidal, e-print arXiv:0711.3960.
[25] Y.-Y. Shi, L.-M. Duan, and G. Vidal, Phys. Rev. A **74**, 022320 (2006).